

PROBING MASSIVE STARS AROUND GAMMA-RAY BURST PROGENITORS

WENBIN LU AND PAWAN KUMAR

Department of Astronomy, University of Texas at Austin, Austin, TX 78712, USA

AND

GEORGE F. SMOOT

PCCP; APC, Université Paris Diderot, Université Sorbonne Paris Cité, 75013 France and
BCCP; LBNL & Physics Dept. University of California at Berkeley CA 94720, USA

Draft version December 3, 2024

ABSTRACT

Long Gamma-Ray Bursts (GRBs) are produced by ultra-relativistic jets launched from core collapse of massive stars. Most massive stars form in binaries and/or in star clusters, which means that there may be a significant external photon field (EPF) around the GRB progenitor. We calculate the inverse-Compton scattering of EPF by the hot electrons in the GRB jet. Three possible cases of EPF are considered: the progenitor is (*I*) in a massive binary system, (*II*) surrounded by a Wolf-Rayet-star wind, and (*III*) in a dense star cluster. Typical luminosities of $10^{47} - 10^{50}$ *erg/s* in the 10 - 100 *GeV* band are expected, depending on the stellar luminosity, binary separation (*I*), wind mass loss rate (*II*), stellar number density (*III*), etc. We calculate the lightcurve and spectrum in each case, taking fully into account the equal-arrival time surfaces and possible pair-production absorption with the prompt γ -rays. Observations can put constraints on the existence of such EPFs (and hence on the nature of GRB progenitors) and on the radius where the jet internal dissipation process accelerates electrons.

Subject headings: Gamma rays: general—Radiation mechanisms: Inverse Compton radiation

1. INTRODUCTION

Long Gamma-Ray Bursts (GRBs) are produced by ultra-relativistic jets launched after the collapse of massive stars (e.g. Galama et al. 1998; Hjorth et al. 2003; Piran 2004; Woosley & Bloom 2006). Massive stars tend to form in binaries and/or in dense star clusters (Massey & Hunter 1998; Zinnecker & Yorke 2007; Mason et al. 2009; Portegies Zwart et al. 2010), which produce a dense external photon field (EPF) around the GRB progenitor. Soft photons will be inverse-Compton (IC) scattered by electrons in the jet. The scattering will boost the energy of photons by a factor of $\Gamma^2 \gamma_e^2$, where $\Gamma \sim 300$ is the jet bulk Lorentz factor (LF) and $\gamma_e \sim 100$ is electrons' LF in the comoving frame. Therefore, we expect EPF at 10 *eV* being scattered to 10's of *GeV*.

In the GRB literature, this external inverse-Compton (EIC) emission is considered for a variety of sources of soft photons and scattering electrons. For example, the soft photons may come from a pulsar wind bubble created before the GRB (Guetta & Granot 2003), and from the funnel of the collapsing star created during the jet breakout (Lazzati et al. 2000; Ghisellini et al. 2000; MacFadyen et al. 2001). Ramirez-Ruiz (2004) considered soft photons from a companion star being IC scattered by a magnetically driven relativistic wind from a spinning-down millisecond supra-magnetar. Giannios (2008) considered the GRB external shock interacting with the photon field from an O star in the surrounding dense cluster.

Different from previous studies, we consider three cases where significant EPFs exist: the GRB progenitor

(*I*) is in a massive binary system, (*II*) has a strong wind, and (*III*) is in a dense star cluster.

In *Case (I)*, soft photons come from a massive companion star. Spectroscopic and direct imaging studies of Galactic massive stars, although biased by selection effects and measurement limitations, conclude that massive stars have binary fraction of at least $\sim 50\%$ (see Mason et al. 2009, and reference therein). Therefore, a companion of comparable mass may exist near the GRB progenitor, depending on the evolution status of the binary system (Langer 2012). For binary separation $d = 10^{15}$ *cm* and the companion star's bolometric luminosity $L_b = 10^{39}$ *erg/s*, the number of scattered photons will be $10^{52} - 10^{53}$ (isotropic equivalent).

In *Case (II)*, soft photons originally from the progenitor star are scattered first by the electrons in the stellar wind and again by the jet. A compact Wolf-Rayet (W-R) star progenitor is favored by considering the propagation time of a GRB jet in the stellar envelope (Matzner 2003). W-R stars have high luminosities of $\sim 10^{39}$ *erg/s* and are surrounded by strong stellar wind of a typical mass loss rate $10^{-5} M_\odot/\text{yr}$ (Crowther 2007). The number of scattered photons is $10^{50} - 10^{51}$ (isotropic equivalent).

In *Case (III)*, all the stars in the cluster create a nearly isotropic and uniform EPF around the GRB jet. Massive stars form in clustered environments (Lada & Lada 2003). In our Galaxy, $\sim 85\%$ of O stars are either observed in young clusters or directly identified as runaways (see Portegies Zwart et al. 2010, and reference therein). Within the central ~ 0.2 *pc* of Arches Cluster, the densest known young massive cluster in the Milky Way, the number density of massive ($30 < M/M_\odot < 120$) stars is ~ 5000 *pc*⁻³ (Espinoza et al. 2009). These stars have luminosities close to or

higher than 10^{39} erg/s. Long GRBs are associated with actively star-forming galaxies (Fruchter et al. 2006; Woosley & Bloom 2006), where young massive clusters are particularly abundant (Portegies Zwart et al. 2010). Therefore, we expect a good fraction, depending on the clusters' evolution, of long GRBs to happen in such star clusters. We consider EIC emission from both internal and external shock in this *Case*. Note that our model is different from Giannios (2008), who consider the case when the external forward shock happen to sweep across one star in the cluster.

In this paper, we show that all three cases may have observable consequences, which can be used to probe massive stars around GRB progenitors and the nature of GRB progenitors.

A few more notes. (1) We call the internal dissipation mechanism that produces the prompt γ -rays as “internal shock” (IS) only for simplicity, but our model is independent of this mechanism (see Kumar & Zhang 2014, for a recent review). (2) The opening angle of the jet is assumed to be larger than the causally connected cone, i.e. $\theta_{j,max} > 1/\Gamma$, so we use the isotropic equivalent energy, luminosity, photon number, etc throughout the paper. (3) The jet is assumed to be hadron dominated and made of pure protons and electrons¹. (4) The convention $X_n = X/10^n$ in CGS units is adopted.

This paper is organized as follows. In Section 2, we give a general treatment of the EIC emission (spectrum and lightcurve) when a jet interacts with an arbitrary EPF. In Section 3, we first give simple order-of-magnitude estimates of the total EIC energy in the three cases, and then put the specific EPFs into the general procedures and calculate the precise lightcurves and spectra. In Section 4, we discuss some potential issues, e.g. absorption of high energy γ -rays by the cosmic background light or by the local EPF itself. Short conclusion is given in Section 5.

2. MODELING THE EIC EMISSION

In this section, we provide a general calculation for the lightcurve and spectrum expected for an observer on the jet axis, when a relativistic jet makes its way through an arbitrary external photon field (EPF).

Such EIC emission has been studied extensively in the literature, for instance for active galactic nuclei (e.g. Dermer & Schlickeiser 1993) where a jet meets an EPF. We refer the readers to Blumenthal & Gould (1970); Aharonian & Atoyan (1981) for a general treatment about IC radiation. Also, Fan et al. (2008) give a review of IC radiation in GRB afterglows, including EIC and synchrotron-self Compton (SSC) radiation. Our treatment is different only in that, at an early stage, equal-arrival time surfaces are taken into consideration. Experienced readers could skip Section 2 and go to Section 3 for the results.

For all the denotations, we use un-primed quantities

¹ Hadrons carry the momentum of the jet but are neglected in the IC scattering process (since there is an equal amount of electrons). If the jet is magnetically dominated, we expect the EIC emission from the internal shock to be much weaker, due to a much smaller number of electrons. For a multi-element jet, e.g. Hydrogen and Helium, our model can be easily modified by putting a $(1 + X(H))/2$ factor before E_j (the total kinetic energy of the jet), where $X(H)$ is the mass fraction of Hydrogen.

in the lab frame (rest frame of the progenitor star) and primed (') ones in the jet comoving frame, and quantities with subscript “j”, e.g. (θ_j, ϕ_j) , are related to different regions in the jet.

As shown in Fig.(1), the jet is moving with a Lorentz factor (LF) Γ in the z direction at radius r . For a volume element (orange) at position $\vec{r} = (r, \theta_j, \phi_j)$, our goal is to consider all the EPF that is scattered into the observer's cone $\Delta\Omega_{obs}$, which is a very small solid angle in the z direction considering the cosmological distances². The EPF specific intensity is denoted as $I_{\nu_0}(\vec{r}, \theta, \phi)$, where \vec{r} is the position of the volume element and (θ, ϕ) is the direction in which photons are moving.

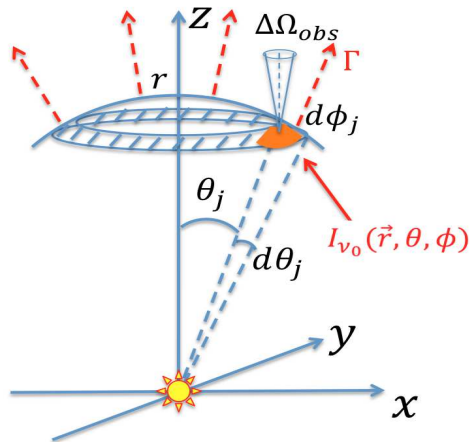


FIG. 1.— Lab frame (progenitor's rest frame). A spherically capped jet is moving in the z direction with bulk Lorentz factor Γ . We consider a small volume element (orange) $r^2 d\Omega_j dr = r^2 \sin\theta_j d\theta_j d\phi_j dr$ of the jet at position $\vec{r} = (r, \theta_j, \phi_j)$. The external photon field at position \vec{r} is denoted by intensity $I_{\nu_0}(\vec{r}, \theta, \phi)$, where (θ, ϕ) is photons' moving direction. Photons scattered into the observer's cone $\Delta\Omega_{obs}$ are considered as observed.

In the comoving frame of the volume element, the observer's cone is

$$\Delta\Omega'_{obs} = \Delta\Omega_{obs}/D_j^2 \quad (1)$$

where D_j is the Doppler factor

$$D_j = \Gamma(1 - \beta \cos\theta_j) \quad (2)$$

and $\beta = \sqrt{1 - 1/\Gamma^2}$ is the velocity of the jet.

Fig.(2) shows the geometry of the comoving frame, where z' axis is aligned with the original moving direction of the volume element. We orient the x' axis in a way that the observer's cone is in the $x'z'$ plane and at an angle θ'_{obs} with the z' axis. Recall that in the lab frame, θ_j is the angle between observer's cone (same as z axis) and the moving direction of the volume element. Therefore, Lorentz transformation (LT) gives

$$\cos\theta'_{obs} = \frac{\cos\theta_j - \beta}{1 - \beta \cos\theta_j} \quad (3)$$

² When calculating the isotropic equivalent luminosity, we use $\Delta\Omega_{obs} = 4\pi$. In this paper, we ignore the cosmological redshift factors, which can be easily included in the final expressions for luminosity, energy, etc. Also, the “comoving frame” means comoving with the jet particles rather than the progenitor's redshift.

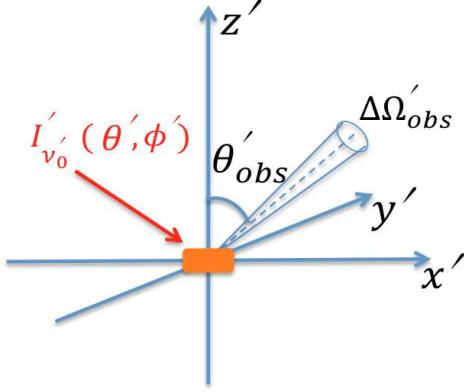


FIG. 2.— Comoving frame of the volume element (orange) in Fig.(1). External photon field is denoted by intensity $I'_{\nu'_0}(\theta', \phi')$. The observer's cone $\Delta\Omega'_{obs}$ is in the $x'z'$ plane. Photons scattered into $\Delta\Omega'_{obs}$ are considered as observed.

Going from $I_{\nu_0}(\theta, \phi)$ to $I'_{\nu'_0}(\theta', \phi')$ needs an axis rotation and a LT. The axis rotation from xyz frame to $\tilde{x}\tilde{y}\tilde{z}$ frame, in which \tilde{z} axis points towards the moving direction, can be expressed by

$$(\vec{e}_1, \vec{e}_2, \vec{e}_3) = R_{\tilde{y}}(\theta_j)R_{\tilde{z}}(\pi - \phi_j)(\vec{e}_1, \vec{e}_2, \vec{e}_3) \quad (4)$$

where $\{\vec{e}_i\}$ and $\{\tilde{e}_i\}$ ($i = 1, 2, 3$) are respectively the basis vectors in the xyz and $\tilde{x}\tilde{y}\tilde{z}$ frame. $R_{\tilde{y}, \tilde{z}}(\alpha)$ are rotation operators, along \tilde{y} or \tilde{z} axis by an angle α according to the right-hand rule. Therefore, a one-to-one map $(\theta, \phi) \rightarrow (\tilde{\theta}, \tilde{\phi})$ is obtained from Eq.(4). Then LT gives the intensity in the comoving frame

$$I'_{\nu'_0}(\theta', \phi') = \tilde{I}_{\nu_0}(\tilde{\theta}, \tilde{\phi}) \cdot \left(\frac{\nu'_0}{\nu_0}\right)^3 \quad (5)$$

and frequency

$$\nu_0 = \Gamma(1 + \beta \cos\theta')\nu'_0 \quad (6)$$

and direction

$$\cos\tilde{\theta} = \frac{\cos\theta' + \beta}{1 + \beta \cos\theta'}, \quad \tilde{\phi} = \phi' \quad (7)$$

In the comoving ($x'y'z'$) frame, if electrons are assumed to be moving isotropically with LF γ_e , the (average) differential IC cross section from (ν'_0, θ', ϕ') to $(\nu', \theta'_{obs}, \phi' = 0)$ is³ (Aharonian & Atoyan 1981)

$$\frac{\partial^2 \sigma}{\partial \nu' \partial \Omega'} \simeq \frac{3\sigma_T}{16\pi\gamma_e^2\nu'_0} \left[1 + \frac{z^2}{2(1-z)} - \frac{2z}{b_\theta(1-z)} + \frac{2z^2}{b_\theta^2(1-z)^2} \right] \quad (8)$$

where $z = h\nu'/(\gamma_e m_e c^2)$, $b_\theta = 2(1 - \cos\theta'_{ic})\gamma_e h\nu'_0/(m_e c^2)$, $h\nu'_0 \ll h\nu' \leq \gamma_e m_e c^2 b_\theta/(1 + b_\theta)$, θ'_{ic} is the angle between the direction of incident and scattered photons, i.e. $\cos\theta'_{ic} = \sin\theta'_{obs}\cos\phi'\sin\theta' + \cos\theta'_{obs}\cos\theta'$, m_e is electron mass, c is speed of light, and σ_T is Thomson cross section.

We consider a powerlaw distribution for electrons

$$dn_e \begin{cases} \propto \gamma_e^{-p} d\gamma_e & \text{if } \gamma_e \geq \gamma_i \\ = 0 & \text{otherwise} \end{cases} \quad (9)$$

³ The approximation is good if $\gamma_e \gg 1$.

Therefore, the averaged differential cross section (ADCS) becomes

$$\begin{aligned} \left\langle \frac{\partial^2 \sigma}{\partial \nu' \partial \Omega'} \right\rangle_{\gamma_e} &= \frac{\int_{\gamma_i}^{\infty} \frac{\partial^2 \sigma}{\partial \nu' \partial \Omega'} \gamma_e^{-p} d\gamma_e}{\int_{\gamma_i}^{\infty} \gamma_e^{-p} d\gamma_e} \\ &= (p-1) \left(\frac{\gamma_i m_e c^2}{h\nu'} \right)^{p+1} \frac{3\sigma_T}{16\pi h\nu'_0 \gamma_i^2} \\ &\cdot \int_0^{z_{max}} \left[1 + \left(\frac{1}{2} - \frac{2}{a_\theta} \right) \frac{z^2}{1-z} + \frac{2}{a_\theta^2} \frac{z^4}{(1-z)^2} \right] z^p dz \end{aligned} \quad (10)$$

where $a_\theta = 2(1 - \cos\theta'_{ic})h^2\nu'_0\nu'/(m_e c^2)^2$, $z_{max} = \min(h\nu'/(\gamma_i m_e c^2), (\sqrt{a_\theta^2 + 4a_\theta} - a_\theta)/2)$. Note that $a_\theta \simeq h^2\nu'_0\nu'/(m_e c^2)^2$ is roughly the criterion for whether EIC scattering is in the Klein-Nishina (KN) regime.

In the low energy band $\nu'/(\gamma_i^2\nu'_0) < 1$, ADCS $\propto \nu'^0$ (i.e. constant), so we expect $\nu' L_{\nu'} \propto \nu'^2$. In the high energy band $\nu'/(\gamma_i^2\nu'_0) > 1$, we have

$$\begin{aligned} z_{max} &= \left(\sqrt{a_\theta^2 + 4a_\theta} - a_\theta \right) / 2 \\ &= \begin{cases} 1 - 1/a_\theta + O(1/a_\theta^2) & \text{if } a_\theta \gg 1 \\ \sqrt{a_\theta} + O(a_\theta) & \text{if } a_\theta \ll 1 \end{cases} \end{aligned} \quad (11)$$

Then we get

$$\left\langle \frac{\partial^2 \sigma}{\partial \nu' \partial \Omega'} \right\rangle_{\gamma_e} \propto \begin{cases} \nu'^{-(p+1)/2} & \text{if } a_\theta \ll 1 \\ \nu'^{-(p+1)} (\ln(a_\theta) + C) & \text{if } a_\theta \gg 1 \end{cases} \quad (12)$$

as pointed out by Blumenthal & Gould (1970) and Aharonian & Atoyan (1981). Therefore, in the Thomson regime ($a_\theta \ll 1$), we expect $\nu' L_{\nu'} \propto \nu'^{(3-p)/2}$; in the KN regime ($a_\theta \gg 1$), we expect $\nu' L_{\nu'} \propto \nu'^{1-p}$. However, as we shall see in Section 3.2, the EIC spectrum is almost never $\nu'^{(3-p)/2}$ or ν'^{1-p} . The reasons are as follows: (1) When $\nu/(\Gamma^2\gamma_i^2\nu_0) < 1$, we are generally in the Thomson regime, and hence we get $\nu L_\nu \propto \nu^2$. (2) When $\nu/(\Gamma^2\gamma_i^2\nu_0) > 1$, we almost immediately get into the KN regime ($a_\theta > 1$), and the $(\ln(a_\theta) + C)$ factor can't be ignored until $a_\theta \geq 100$ (i.e. $h\nu \geq 3 \text{ TeV}$). As the high energy tail suffers from pair-production absorption (see the Appendix), the spectra hardly reach TeV band.

Suppose the volume element (orange in Fig.1) contains dN_e electrons, the number of photons that are scattered into $\Delta\Omega'_{obs}$, in a time duration dt' and frequency range $d\nu'$, is

$$\begin{aligned} dN_\gamma &= dN_e \cdot \left\langle \frac{\partial^2 \sigma}{\partial \nu' \partial \Omega'} \right\rangle_{\gamma_e} d\nu' \Delta\Omega'_{obs} \\ &\cdot \int_{4\pi} d\Omega' \int_0^\infty d\nu'_0 \frac{I'_{\nu'_0}(\theta', \phi')}{h\nu'_0} e^{-\tau(\nu'_0, \theta')} dt' \end{aligned} \quad (13)$$

where the optical depth τ describes the attenuation by the part of the jet that lies along the incident photons' trajectory before they enter the jet volume element where its IC scattering is considered. We assume the jet is launched steadily with (isotropic) power L_j and duration T_j , total (isotropic) kinetic energy is E_j , and the

thickness of the jet is $\Delta r = cT_j$. Photons are all assumed to enter the jet from the front surface, which is at radius r . If the volume element is located δr from the jet front, the optical depth along the incident photons' trajectory is

$$\tau(\nu'_0, \theta') = \frac{\delta r}{\Delta r} \frac{E_j}{\Gamma m_p c^2} \sigma_{tot}(\nu'_0) \cdot \frac{1}{4\pi r^2 |\cos\theta'|} \quad (14)$$

where $|\cos\theta'|$ is due to the incident angle onto the front surface and $\sigma_{tot}(\nu'_0)$ is given by

$$\sigma_{tot}(\nu'_0) = \int_0^\infty d\nu' \int_{4\pi} d\Omega' \left\langle \frac{\partial^2 \sigma}{\partial \nu' \partial \Omega'} \right\rangle_{\gamma_e} \quad (15)$$

i.e. the (γ_e -averaged) total cross section of one electron for photons at frequency ν'_0 .

Actually, not all the dN_γ (Eq.13) photons will be observed. Photons of energy $h\nu \gtrsim 10 \text{ GeV}$ may collide with low energy photons (such as the GRB prompt emission) and produce pairs. In the Appendix, we calculate the pair-production optical depth $\tau_{\gamma\gamma}(\nu, r)$ (Eq.A9) for high energy photons produced at radius r and have frequency ν . Basically, we show that only the absorption by the GRB prompt emission may be important. And we use a broken powerlaw spectrum (Band et al. 1993) with low (high) frequency index -1 (-2.4), break frequency 200 keV and bolometric isotropic luminosity 10^{52} erg/s , following the Fermi GRB statistics (Gruber et al. 2014). Then, the dN_γ in Eq.(13) is multiplied by $e^{-\tau_{\gamma\gamma}}$.

Next we include the effect of the conical shape of the jet ("curvature effect") on the observed luminosity. Scattered photons from a volume element at δr from the jet front and at latitude θ_j will arrive at observer's time $t_{obs}(\delta r, \theta_j)$. Photons arriving at the same time are from the same equal-arrival time surface, described by

$$r_{eq}(\theta_j, \delta r, t_{obs}) = \delta r + \beta \frac{ct_{obs} - \delta r}{1 - \beta \cos\theta_j} \quad (16)$$

We divide the jet into many thin shells of thickness $d(\delta r)$ according to the distance to the jet front δr and calculate the lightcurve contributed by each shell. Using Lorentz transformation in time $dt' = dr_{eq}/(\Gamma c) \simeq dt_{obs}/D_j$ and frequency $\nu' = D_j \nu$ in Eq.(13), we obtain the specific luminosity from one shell $d(\delta r)$ at δr

$$\begin{aligned} dL_\nu &= \frac{dN_\gamma h\nu}{dv dt_{obs}} e^{-\tau_{\gamma\gamma}(\nu, r)} \\ &= \frac{E_j}{\Gamma m_p c^2} \frac{d(\delta r)}{\Delta r} \frac{\int d\Omega_j}{4\pi} \frac{h\nu \Delta\Omega_{obs}}{D_j^2} \cdot \left\langle \frac{\partial^2 \sigma}{\partial \nu' \partial \Omega'} \right\rangle_{\gamma_e} \\ &\cdot e^{-\tau_{\gamma\gamma}(\nu, r)} \cdot \int_{4\pi} d\Omega' \int_0^\infty d\nu'_0 \frac{I'_{\nu'_0}(\theta', \phi')}{h\nu'_0} e^{-\tau(\theta')} \end{aligned} \quad (17)$$

where $\int d\Omega_j = \int_0^{\theta_{j,max}} \sin\theta_j d\theta_j \int_0^{2\pi} d\phi_j$ and we use $\theta_{j,max} = 2/\Gamma$ (not sensitive) in our numerical results (Section 3.2). Then, the total observed luminosity is obtained by adding up all the shells, i.e. integrating Eq.(17) over $\int_0^{\Delta r} d(\delta r)$.

3. APPLICATIONS

In this section, we apply the procedures developed in Section 2 to three different cases, where the EPFs

are given by the physical environment. First, in Section 3.1, we give simple order-of-magnitude estimates of the total EIC energy, not considering the pair production. See Tab.(1) for the summary of our estimates on peak frequency, EIC luminosity, duration, etc in all cases. Then in Section 3.2, we present the precise lightcurves and spectra, with absorption from pair production (with prompt γ -rays) considered.

3.1. Order-of-magnitude Estimate

3.1.1. Case (I) — Binary System

Consider the GRB progenitor star being in a binary system. Soft photons from the companion star are scattered by the electrons in the GRB relativistic jet.

We assume the direction of the jet is perpendicular to the orbital plane⁴. As shown in Fig.(3), the jet is at a distance r from the progenitor star (A) and is moving with LF Γ in the z direction, and the companion star (B) is on the x axis at a distance d from A. Photons from Star B encounter the jet at an angle $\cos\theta_* = r/\sqrt{r^2 + d^2}$.

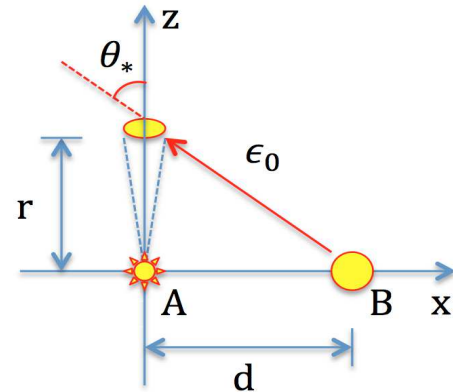


FIG. 3.— Geometry of Case (I). The jet is on the z axis at a distance r from the progenitor star (A). The companion star (B) is on the x axis at a distance d from Star A. Photons from Star B encounter the jet at an angle $\cos\theta_* = r/\sqrt{r^2 + d^2}$.

Suppose the companion star has a bolometric luminosity $L_b = 10^{39} \text{ erg/s}$ $L_{b,39}$ and peak energy $\epsilon_0 = 10 \text{ eV}$ $\epsilon_{0,1}$. Considering the recoil of electrons in the Compton interaction, we estimate the energy of scattered photons by

$$\begin{aligned} \epsilon &\simeq \min(\Gamma^2 \gamma_e^2 \epsilon_0, \Gamma \gamma_e m_e c^2) \\ &= 9 \text{ GeV} \Gamma_{2.5}^2 \gamma_{e,2}^2 \epsilon_{0,1} \eta_{KN} \end{aligned} \quad (18)$$

where we have used fiducial LFs $\Gamma = 300 \Gamma_{2.5}$, $\gamma_e = 10^2 \gamma_{e,2}$, and

$$\eta_{KN} = \min\left(1, \frac{1.7}{\Gamma_{2.5} \gamma_{e,2} \epsilon_{0,1}}\right) \quad (19)$$

describes the degree to which EIC scattering is KN suppressed. Suppose the jet is launched steadily with (isotropic) power $L_j = 10^{53} \text{ erg/s}$ $L_{j,53}$ and duration $T_j = 10 \text{ s}$ $T_{j,10}$, so the total (isotropic) kinetic energy

⁴ Even if the jet direction is inclined by up to 30° from the normal direction of orbital plane, the total energy (or luminosity) will be affected by a factor of order unity ($\lesssim 2$).

is $E_j = 10^{54} \text{erg}$ $E_{j,54}$ and the thickness of the jet is $\Delta r = cT_j = 3 \times 10^{11} \text{cm}$ $T_{j,1}$. Considering KN suppression, we estimate the EIC optical depth of the whole jet as

$$\tau_j(r) \simeq \frac{E_j \sigma_T}{4\pi r^2 \Gamma m_p c^2} \eta_{KN} \quad (20)$$

The jet becomes transparent at radius

$$r_{tr} \simeq 3.4 \times 10^{14} \text{cm} \sqrt{\frac{E_{j,54}}{\Gamma_{2.5}} \eta_{KN}} \quad (21)$$

The number density of EPF is given by

$$n_\gamma = \frac{L_b}{4\pi(r^2 + d^2)\epsilon_0 c} \quad (22)$$

The total (isotropic) number of scattered photons is

$$N_\gamma = \int_0^\infty (1 - \beta \cos \theta_*) n_\gamma(r, d) \min(1, \tau_j(r)) 4\pi r^2 dr \quad (23)$$

from which, we can easily see that most photons are scattered at radius $r \sim d$. Therefore, we can estimate

$$N_\gamma \sim 3 \times 10^{53} \frac{L_{b,39} d_{15}}{\epsilon_{0,1}} \min\left(1, \frac{r_{tr}^2}{d^2}\right) \quad (24)$$

Multiplying N_γ by the scattered photons' energy from Eq.(18), we get the total EIC energy

$$E_{EIC} \sim 4 \times 10^{51} \text{erg} \Gamma_{2.5}^2 \gamma_{e,2}^2 \eta_{KN} L_{b,39} d_{15} \min\left(1, \frac{r_{tr}^2}{d^2}\right) \quad (25)$$

Note that the estimate is not accurate when $r_{tr} \gg d$, because the soft photons are moving nearly parallel to jet, and hence both N_γ and ϵ decrease by orders of magnitude.

3.1.2. Case (II) — Stellar Wind

As suggested by e.g. Woosley (1993) and MacFadyen & Woosley (1999), GRB progenitor stars are possibly Wolf-Rayet (W-R) stars, which have a typical mass loss rate of $10^{-5} M_\odot/\text{yr}$, bolometric luminosity 10^{39}erg/s , and effective temperature 10^5K (Crowther 2007). We consider that photons originally from the progenitor star are scattered first by the wind and then by the jet. The geometry is shown in Fig.(4).

We assume a steady wind and denote the wind velocity⁵ as $v = 10^8 \text{cm/s}$ v_8 and the mass loss rate as $\dot{M} = 10^{-5} M_\odot/\text{yr}$ \dot{M}_{-5} . The wind-scattering optical depth of the region with radius $> r$ is

$$\begin{aligned} \tau_{wind}(r) &= \sigma_T \int_r^\infty \frac{\dot{M}}{4\pi \tilde{r}^2 v m_p c^2} d\tilde{r} \\ &\simeq 2 \times 10^{-3} \frac{\dot{M}_{-5}}{v_8} r_{14}^{-1} \end{aligned} \quad (26)$$

Therefore, the wind-scattered photon density is

$$n_\gamma(r) = \frac{L_b \tau_{wind}(r)}{4\pi r^2 \epsilon_0 c} (\propto r^{-3}) \quad (27)$$

⁵ The order of escape velocity.

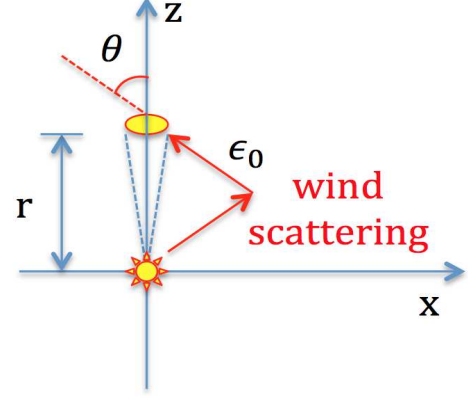


FIG. 4.— Geometry of Case (II). The jet is on the z axis at a distance r from the progenitor star. Photons originally from Star A are scattered first by electrons in the wind and again by the jet. The wind scattered photons encounter the jet with an angle θ .

The number of scattered photons has a logarithmic dependence on r when $r < r_{tr}$, and then drops off as r^{-2} at larger radius, so we can estimate the total (isotropic) number of scattered photons as

$$N_\gamma = 2.9 \times 10^{51} \frac{L_{b,39} \dot{M}_{-5}}{\epsilon_{0,1} v_8} \ln\left(\frac{r_{tr,14}}{R_{*,11}}\right) \quad (28)$$

where $R_* = 10^{11} \text{cm}$ $R_{*,11}$ is the radius of the star. Therefore, the total EIC energy is

$$E_{EIC} = 4.2 \times 10^{49} \text{erg} \frac{L_{b,39} \dot{M}_{-5} \Gamma_{2.5}^2 \gamma_{e,2}^2 \eta_{KN}}{v_8} \ln\left(\frac{r_{tr,14}}{R_{*,11}}\right) \quad (29)$$

3.1.3. Case (III) — Star Cluster

Consider that the GRB progenitor star is in a young massive cluster. All the stars in the cluster create a nearly isotropic and uniform EPF around the GRB jet. Scatterings by electrons accelerated by both internal shock (IS) and external shock (ES) may be important. We assume that the cluster has a (O-)star density of $n_* = 10^4 \text{pc}^{-3}$ $n_{*,4}$ and a radius of $R = 1 \text{pc}$ R_{pc} . We assume stars have an average bolometric luminosity of $L_b = 10^{39} \text{erg/s}$ $L_{b,39}$ and peak energy $\epsilon_0 = 10 \text{eV}$ $\epsilon_{0,1}$. The number density of EPF can be estimated as

$$n_\gamma \simeq \frac{n_* L_b R}{\epsilon_0 c} \simeq 2 \times 10^6 \text{cm}^{-3} \frac{n_{*,4} L_{b,39} R_{pc}}{\epsilon_{0,1}} \quad (30)$$

First, we consider IS. After the jet becomes transparent, $4\pi r^2 n_\gamma \tau_j$ is a constant. The total number of scattered photons depends on the largest radius where electrons stay hot r_{max} , which is quite uncertain (Piran 2004; Mészáros 2006; Kumar & Zhang 2014). Observationally, the duration of GRB prompt emission ($T_{90}/(1+z) \sim 10 \text{s}$) gives an upper limit of the radius where the IS is active

$$r_{IS} \leq 2\Gamma^2 c T_{90}/(1+z) \simeq 5 \times 10^{16} \text{cm} \Gamma_{2.5}^2 \quad (31)$$

Theoretically, an upper limit of r_{IS} is the deceleration radius r_{dec} (see Eq.37 below), where the jet starts to decelerate substantially. Note that, after the prompt emission is produced, electrons cool via adiabatic expansion

TABLE 1

Cases	$I (d = 10^{14})$	$I (d = 10^{15})$	$I (d = 10^{16})$	II	III (IS)	III (RS)	III (FS)
$h\nu_p$ [GeV]	9	9	9	9	9	9	26
L_{EIC}^{iso} [erg/s]	4×10^{49}	5×10^{49}	5×10^{48}	5×10^{48}	10^{49}	5×10^{48}	2×10^{46}
t_{obs} [s]	10	10	10	10	10	2×10^2	2×10^4
$N_{EIC}^{iso} (*)$	3×10^{52}	3×10^{52}	3×10^{51}	3×10^{51}	10^{52}	10^{53}	6×10^{51}
$r_{eff} (**)$ [cm]	$d(10^{14})$	$d(10^{15})$	$d(10^{16})$	$r_{tr}(3 \times 10^{14})$	$r_{max}(10^{16})$	$r_{dec}(10^{17})$	$r_{KN}(3.3 \times 10^{17})$
$e^{-\tau_{\gamma\gamma}} (***)$	0.06	0.4	0.7	0.2	0.8	1	1

NOTE. — Summary of the EIC emission from our analytical calculation (Section 3.1, not considering pair-production absorption), including $h\nu_p$ (**peak energy**), L_{EIC}^{iso} (**isotropic EIC luminosity**), N_{EIC}^{iso} (**isotropic number of EIC photons**), t_{obs} (**duration of EIC emission**). The scaled parameters are all set to 1, including $E_{j,54}$ (isotropic jet kinetic energy), $T_{j,1}$ (jet duration), $\Gamma_{2.5}$ (jet bulk LF), $\gamma_{e,IS,2}$ (IS-accelerated electrons' LF), $r_{max,16}$ (the maximum radius electrons stay hot), $\Gamma_{dec,2}$ (bulk LFs of FS and RS at deceleration radius), $\gamma_{e,RS,2.5}$ (RS-accelerated electrons' LF), $r_{dec,17}$ (deceleration radius), $T_{4,7}$ (temperature of EPF-contributing stars), $L_{b,39}$ (bolometric luminosity of EPF-contributing stars), \dot{M}_{-5} (wind mass loss rate), v_8 (wind velocity), $n_{*,4}$ (stellar number density in the cluster), R_{pc} (radius of the cluster).

(*) — 10^{52} photons from 1 Gpc ($z = 0.25$) give a photon fluence of 10^{-4} cm^{-2} .

(**) — By using a constant γ_e at all radius (i.e. no dynamical evolution) in our analytical and numerical calculations, we are making an assumption that electrons are hot near the radius r_{eff} where most scatterings happen (see Fig.6 for a justification).

(***) — The pair-production absorption caused by prompt γ -rays, for which we used an isotropic luminosity $L_\gamma = 10^{52} \text{ erg/s}$, Band-function low energy index $\alpha_1 = -1$, high energy index $\alpha_2 = -2.4$ and break frequency $h\nu_b = 200 \text{ keV}$. Specifically, we calculate from our numerical results (see Section 3.2) $e^{-\tau_{\gamma\gamma}} = N_{EIC,a}^{iso}/N_{EIC}^{iso}$, i.e. the ratio of isotropic number of EIC photons when the absorption is/isn't considered. We can see that absorption is (not) significant at radius smaller (greater) than 10^{15} cm .

$\gamma_e \propto r^{-2/3}$ and may stay hot for some time. Putting the uncertainties in the parameter $r_{max} = 10^{16} \text{ cm}$ $r_{max,16}$, we estimate the total EIC energy by

$$\begin{aligned}
 E_{EIC} &\simeq (\epsilon\tau_j n_\gamma 4\pi r^3/3)|_{r=r_{max}} \\
 &\simeq 1.4 \times 10^{50} \text{ erg } E_{j,54} \Gamma_{2.5} \gamma_{e,2}^2 \eta_{KN}^2 \quad (32) \\
 &\cdot n_{*,4} L_{b,39} R_{pc} \cdot r_{max,16}
 \end{aligned}$$

Next, we consider the EIC emission from ES, where both the reverse shocked (RS) and forward shocked (FS) region may contribute significantly. EIC emission from ES strongly depends on the ES dynamical evolution.

We assume pressure equilibrium⁶ between FS and RS region (Kobayashi 2000), both moving together with LF Γ_{sh} . Then Γ_{sh} is only a function of jet LF Γ and the density ratio n/n_{ej} , where n is the number density of the circum-burst medium and n_{ej} is the comoving number density of unshocked ejecta. Before RS crosses the jet, the LF of the shocked region is (Uhm 2011)

$$\Gamma_{sh}(r) = \frac{\Gamma}{(1 + 2\Gamma\sqrt{n(r)/n_{ej}(r)})^{1/2}} \quad (33)$$

The comoving number density of the unshocked ejecta is

$$n_{ej}(r) = \frac{E_j}{4\pi r^2 T_j \Gamma^2 m_p c^3} \quad (34)$$

The circum-burst medium is either a uniform density medium or stratified like a wind ($n \propto r^{-2}$) out to the

⁶ This may only hold for a so-called short-lived RS, but see Uhm (2011) for a description of a long-lived RS, where RS may reach a much larger radius. Then the EIC energy from RS could be much larger.

wind termination shock radius. GRB afterglow analyses suggest that about half of the long GRBs have a uniform or weak (1/100 W-R) wind density profile, rather than a normal W-R wind profile (e.g. Panaitescu & Kumar 2001; Chevalier et al. 2004), the reason for which is still an open question. For simplicity, we take the electrons' number density in the cluster to be uniform $n = 10 \text{ cm}^{-3} n_1$.

Then we can determine the jet dynamics, which is characterized by the deceleration radius r_{dec} (see e.g. Piran 2004). At radius $r < r_{dec}$, whether RS is relativistic ($\Gamma_{sh} \ll \Gamma$) or Newtonian ($\Gamma_{sh} \approx \Gamma$) depends on the factor in Eq.(33) $2\Gamma(n/n_{ej})^{1/2} \simeq 0.48\Gamma_{2.5}^2 r_{17}^{1/2} (n_1 T_{j,1}/E_{j,54})^{1/2}$. For a fast jet, say $\Gamma \geq 10^3$, from Eq.(33), we have

$$\Gamma_{sh}(r) \simeq 1.4 \times 10^2 r_{17}^{-1/2} \left(\frac{E_{j,54}}{n_1 T_{j,1}} \right)^{1/4} (\ll \Gamma) \quad (35)$$

For a slow jet, say $\Gamma = 100$, $2\Gamma(n/n_{ej})^{1/2} \ll 1$, so we have $\Gamma_{sh}(r \leq r_{dec}) \simeq 100$.

The deceleration radius can be estimated by

$$\Gamma_{sh}^2 \frac{4\pi}{3} r_{dec}^3 n m_p c^2 = E_j/2 \quad (36)$$

which gives

$$r_{dec} \simeq 9.3 \times 10^{16} \text{ cm } \frac{E_{j,54}^{1/3}}{\Gamma_{sh,2}^{2/3} n_1^{1/3}} \quad (37)$$

Therefore, for a jet LF $\Gamma \in (10^2, 10^3)$, we always have $r_{dec} \sim 10^{17} \text{ cm}$ and $\Gamma_{dec} \equiv \Gamma_{sh}(r_{dec}) \sim 100$. Hereafter

we use $r_{dec} = 10^{17} \text{cm}$ $r_{dec,17}$ and $\Gamma_{dec} = 10^2 \Gamma_{dec,2}$ as the fiducial values.

Electrons in the RS and FS region are accelerated to different LFs. Assuming a fraction ϵ_e of the shocked fluid's internal energy goes into electrons, we have

$$\gamma_e \simeq \begin{cases} \epsilon_{e,r} \frac{1}{2} \left(\frac{\Gamma}{\Gamma_{sh}} + \frac{\Gamma_{sh}}{\Gamma} \right) \frac{m_p}{m_e} & \text{(RS)} \\ \epsilon_{e,f} \Gamma_{sh} \frac{m_p}{m_e} & \text{(FS)} \end{cases} \quad (38)$$

where m_p and m_e are proton and electron mass. Below, we consider RS and FS separately.

(1) *RS*: EIC emission from RS peaks when RS crosses the end of the jet. After shock crossing, a rarefaction wave propagates through the RS region at sound speed and decreases the internal energy substantially. Despite the difference between shock crossing time (slightly earlier, typically) and deceleration time (later), a good approximation is that RS region stays hot until r_{dec} . The energy equipartition parameter $\epsilon_{e,r}$ is poorly constrained from GRB afterglows, since there are not many confirmed RS detections. Considering the uncertainties, we use $\epsilon_{e,r} = 0.1$ (the same as in FS). Therefore, from Eq.(38), we get $\gamma_e \simeq 1.8 \times 10^2 (1 + \Gamma/2\Gamma_{sh})$, i.e. typically a few hundred. Hereafter, we use $\gamma_e = 300\gamma_{e,2.5}$ as fiducial value.

According to Eq.(18), the scattered photons' energy is $\epsilon \simeq 9 \text{GeV} \Gamma_{dec,2}^2 \gamma_{e,2.5}^2 \epsilon_{0,1}$ (marginally KN suppressed) and the total (isotropic) EIC energy from RS can be estimated as

$$\begin{aligned} E_{EIC}^{RS} &= (\epsilon \tau_j n_\gamma 4\pi r^3 / 3) |_{r=r_{dec}} \\ &\simeq 1.4 \times 10^{51} \text{erg} \frac{E_{j,54}}{\Gamma_{2.5}} n_{*,4} L_{b,39} R_{pc} \Gamma_{dec,2}^2 \gamma_{e,2.5}^2 r_{dec,17} \end{aligned} \quad (39)$$

(2) *FS*: We use Eq.(38) with a constant $\epsilon_e = 0.1$ (Panaitescu & Kumar 2001) to get electrons' LF. At r_{dec} , EIC radiation from FS region is strongly KN suppressed, so the total EIC energy is rising with r ($E_{EIC}^{FS} \propto r^4$ as shown below), until the scattering changes from KN to Thomson regime. The characteristic radius where this transition happens is denoted as r_{KN} , given by

$$\Gamma_{sh}(r_{KN}) \gamma_e \epsilon_0 = m_e c^2 \quad (40)$$

After r_{dec} , we expect the Blandford-McKee evolution (Blandford & McKee 1976)

$$\Gamma_{sh}(r) \simeq \Gamma_{dec} \left(\frac{r}{r_{dec}} \right)^{-3/2} \quad (41)$$

Putting Eq.(38) and (41) to Eq.(40), we get the ‘‘KN radius’’

$$r_{KN} \simeq 3.3 r_{dec} \Gamma_{dec,2}^{2/3} \epsilon_{0,1}^{1/3} \quad (42)$$

We know $E_{EIC}^{FS} \propto \epsilon \tau_{FS} r^3$. When $r_{dec} < r < r_{KN}$, the scattered photons' energy $\epsilon \propto r^{-3}$, and the optical depth of FS region $\tau_{FS} \propto r^4$, so we get $E_{EIC}^{FS} \propto r^4$. In a similar way, when $r > r_{KN}$, we get $E_{EIC}^{FS} \propto r^{-2}$. Therefore, most EIC emission is produced at radius r_{KN} ,

and we obtain

$$\begin{aligned} E_{EIC}^{FS} &\simeq (\epsilon \tau_{FS} n_\gamma 4\pi r^3 / 3) |_{r=r_{KN}} \\ &\simeq 2.6 \times 10^{50} \text{erg} \frac{n_{*,4} L_{b,39} R_{pc}}{\epsilon_{0,1}^{2/3}} n_{17}^4 r_{dec,17} \Gamma_{dec,2}^{8/3} \end{aligned} \quad (43)$$

where we have used $\epsilon(r_{KN}) \simeq (m_e c^2)^2 / \epsilon_0 = 26 \text{GeV} \epsilon_{0,1}^{-1}$ and $\tau_{FS} \simeq r_{KN} n \sigma_T / 3$. We note the strong dependence on both r_{dec} and Γ_{dec} . Also, higher energy (up to $\sim T_e V$) photons are produced at radius $r_{dec} < r < r_{KN}$, but they contribute a smaller EIC energy.

3.2. Lightcurves and Spectra

In this subsection, we put realistic EPF profiles into the procedure developed in Section 2 and calculate the precise lightcurves and spectra for the three cases. As a general assumption, in each case, the star(s) that contribute to EPF are assumed to have bolometric luminosity $L_b = 10^{39} \text{erg/s}$ $L_{b,39}$ and effective temperature $T = 5 \times 10^4 \text{K}$ $T_{4.7}$, so the specific luminosity is

$$L_{\nu_0} = \frac{\pi L_b}{\sigma_{SB} T^4} \cdot \frac{2h\nu_0^3}{c^2} \frac{1}{e^{h\nu_0/kT} - 1} \quad (44)$$

where σ_{SB} is the Stefan-Boltzmann constant.

(I) *Binary Case*: We consider the companion star as a point source, so the EPF intensity at position $\vec{r} = (r, \theta_j, \phi_j)$, in the direction (θ, ϕ) , is

$$I_{\nu_0}(\vec{r}, \theta, \phi) = \frac{L_{\nu_0}}{4\pi(r^2 + d^2)} \sin\theta_* \delta(\theta - \theta_*) \delta(\phi - \pi) \quad (45)$$

where $\sin\theta_* = d/\sqrt{r^2 + d^2}$, d is the binary separation, and $\delta(x)$ is the Dirac- δ function.

(II) *Wind Case*: Assuming a steady wind with mass loss rate \dot{M} and speed v , we get the number density of circum-stellar electrons at a distance r from the center

$$n_e(r) = \frac{\dot{M}}{4\pi r^2 v} \quad (46)$$

Then the emissivity from wind scattering is

$$j_{\nu_0}(r) = \frac{n_e(r) \sigma_T}{4\pi r^2} \cdot L_{\nu_0} \quad (47)$$

which is isotropic (no dependence on θ or ϕ) from Thomson scattering. The system is spherical symmetric, so j_{ν_0} doesn't depend on θ_j or ϕ_j , and hence neither does the intensity I_{ν_0} . Therefore, we can integrate along the (θ, ϕ) direction and get the EPF intensity at position \vec{r}

$$\begin{aligned} I_{\nu_0}(r, \theta, \phi) &= \int_0^\infty j_{\nu_0}(r(s)) ds \\ &= 8.0 \times 10^9 \frac{\dot{M}_5}{v_8} \frac{\pi - \theta + \sin\theta \cos\theta}{\sin^3\theta} \frac{L_{\nu_0}}{r^3} \end{aligned} \quad (48)$$

which is independent of ϕ , due to symmetry. Note that the function $f(\theta) = (\pi - \theta + \sin\theta \cos\theta) / \sin^3\theta \simeq 2(\pi - \theta)^2 / 3 \rightarrow 0$ when $\theta \rightarrow \pi^-$ and $f(\theta) \simeq \theta^{-3} \rightarrow \infty$ (diverges⁷) when $\theta \rightarrow 0^+$. However, photons with $\theta < 1/\Gamma$

⁷ The divergence is caused by the assumption of the star being a point source. If we denote the progenitor star's radius as R_* , at

are moving nearly parallel to the jet and hence don't contribute significantly to the spectra.

(III) *Star Cluster Case*: All the stars in the cluster create a more or less uniform and isotropic EPF, so the intensity can be estimated as

$$I_{\nu_0} \simeq \frac{n_* L_{\nu_0} R_c}{4\pi} \quad (49)$$

where n_* is the number density of stars and R_c is the radius of the cluster.

Below, we present the lightcurves and spectra from the internal shock for the three cases, and discuss the prospects of detecting the predicted high energy photons. The jet bulk LF $\Gamma = 300\Gamma_{2.5}$ is our fiducial value, but the results from $\Gamma = 10^3\Gamma_3$ in each case are also shown for comparison. The other scaled parameters $E_{j,54}$, $T_{j,1}$, $\gamma_{i,2}$, $r_{max,15}$, $\Gamma_{dec,2}$, $r_{dec,17}$, $T_{4.7}$, $L_{b,39}$ are all set to 1. Electrons' LF distribution powerlaw index $p = 2.2$. We first calculate the spectra at observer's time $t_{obs} = 1$ s in *Case (I)* and *(II)*, and $t_{obs} = 10$ s in *Case (III)*. Then we measure the peak frequency ν_p in the spectra. The lightcurves are then calculated at ν_p .

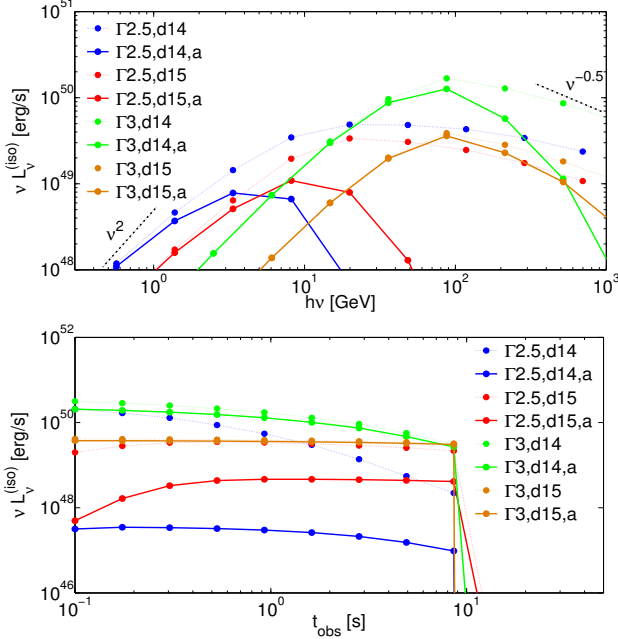


FIG. 5.— Spectra at $t_{obs} = 1$ s (upper panel) and lightcurves at ν_p (lower panel) in the *Binary Case*, under different binary separations d and bulk LFs Γ . We show the differences between calculations with/without pair-production absorption by using dotted/solid lines (“a” means absorption is considered). Absorption is weaker under a larger bulk LF and a larger binary separation. Considering absorption (solid lines), the total EIC energy is $E_{EIC} = 2.4 \times 10^{48}$ (blue), 6.4×10^{49} (red), 8.5×10^{50} (green), and 4.8×10^{50} (brown) erg. The spectra show $\nu L_{\nu} \propto \nu^2$ below ν_p and $\propto \nu^{-0.5}$ above ν_p , plus additional high energy softening caused by absorption. The scaled parameters $E_{j,54}$, $T_{j,1}$, $\gamma_{i,2}$, $T_{4.7}$, $L_{b,39}$ are all set to 1. Powerlaw index $p = 2.2$.

an angle $\theta < \arcsin(R_*/r)$, photons come directly from the star. However, as long as the star is not a giant ($R_* < 10^{13}$ cm), the photons directly from the star are moving nearly parallel to the jet and are hence negligible.

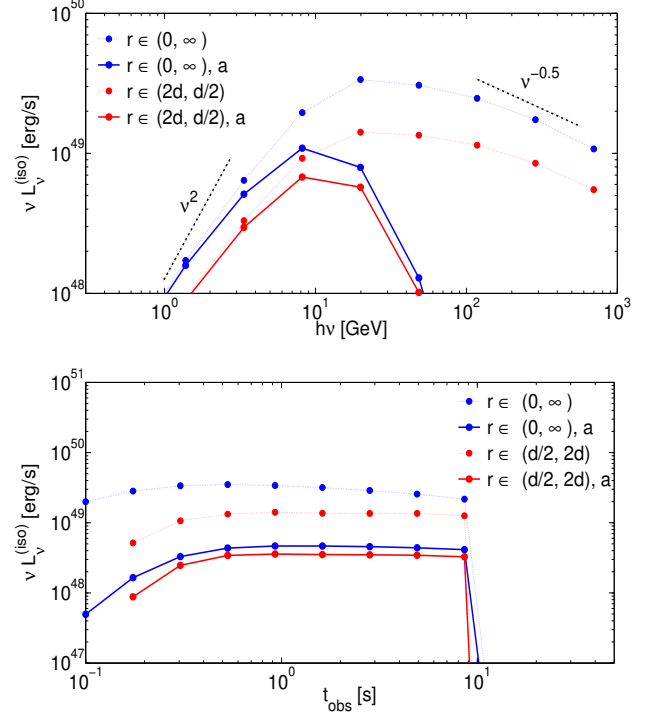


FIG. 6.— The comparison between when electrons are hot in a limited radius range $r \in (d/2, 2d)$ (red) and when electrons are hot at all radius (blue), in the *Binary Case* when d_{15} , $\Gamma_{2.5} = 1$. Calculations with/without pair-production absorption are denoted by dotted/solid lines (“a” means absorption is considered). Considering absorption, the total EIC energy is $E_{EIC} = 6.4 \times 10^{49}$ (blue), 5.0×10^{49} (red) erg. The small difference means that, by using a constant γ_i at all radius, we are making an assumption that electrons are hot near the radius where most scatterings happen (see r_{eff} in Tab.1).

A summary of our numerical results is as follows:

(1) EIC emission is concentrated in 10 - 100 GeV band. The total EIC energy is typically $10^{48} \sim 10^{51}$ erg (hence luminosity $10^{47} \sim 10^{50}$ erg/s) and the photon fluence is $10^{-7} \sim 10^{-5}$ cm^{-2} at redshift $z = 1$.

(2) The numerical spectra follow the scaling of the averaged differential cross section (Eq.10) quite well. Without considering pair production, we get $\nu L_{\nu} \propto \nu^2$ below ν_p and $\propto \nu^{-0.5}$ above ν_p . The spectra become increasingly steeper as we go to higher energy and the expected ν^{1-p} slope only shows up above TeV band. However, pair production usually makes the high energy tail much softer.

(3) The observational challenge is that the EIC emission from the internal shock arrives within ~ 10 s of the GRB trigger, which requires that the GRB occurs in the large field of view of a telescope, e.g. Fermi Large Area Telescope (LAT) (Ackermann et al. 2013), wide-field-mode Cherenkov Telescope Array (CTA) (Inoue et al. 2013). However, in the *Star Cluster Case*, although not shown in the figures, EIC photons from the reverse shock will arrive at deceleration time $t_{dec} = r_{dec}/(2c\Gamma_{dec}^2) \sim 200$ s and those from the

⁸ The luminosity distance $D_{L,z=1} = 2.0 \times 10^{28}$ cm from $D_L = c(1+z)/H_0 \int_0^z dx/\sqrt{\Omega_m(1+x)^3 + \Omega_\Lambda}$, and $\Omega_m = 0.27$, $\Omega_\Lambda = 0.73$, $H_0 = 71$ km s⁻¹ Mpc⁻¹.

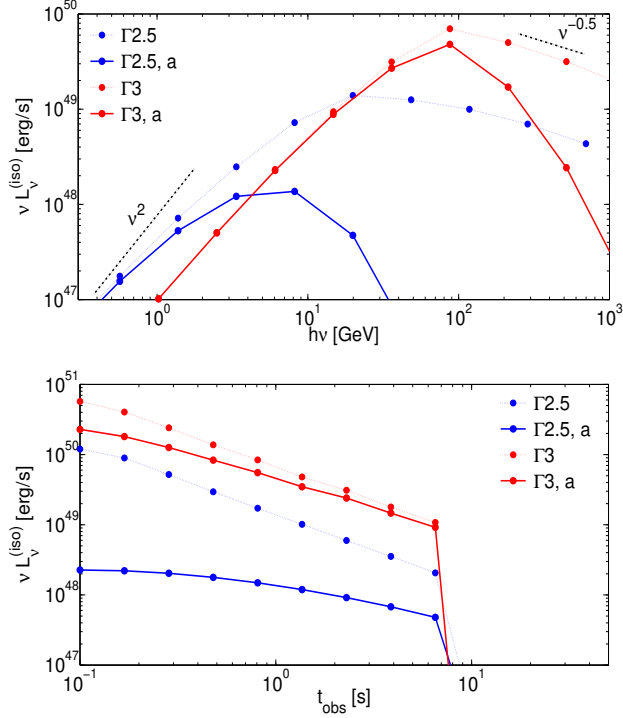


FIG. 7.— Spectra at $t_{obs} = 1$ s (upper panel) and lightcurves at ν_p (lower panel) in the *Wind Case*, under different bulk LFs. We show the differences between calculations with/without pair-production absorption by using dotted/solid lines (“a” means absorption is considered). Absorption is usually strong in this case. Considering absorption (solid lines), the total EIC energy is $E_{EIC} = 8.7 \times 10^{48}$ (blue), 2.7×10^{50} (red) erg. The spectra show $\nu L_\nu \propto \nu^2$ below ν_p and $\propto \nu^{-0.5}$ above ν_p , plus additional high energy softening caused by absorption. The scaled parameters $E_{j,54}$, $T_{j,1}$, $\gamma_{i,2}$, $T_{4,7}$, $L_{b,39}$, \dot{M}_{-5} , v_8 are all set to 1. Powerlaw index $p = 2.2$.

forward shock will arrive at the time when the scattering changes from KN to Thomson regime $t_{KN} = r_{KN}/[2c\Gamma_{sh}(r_{KN})^2] \sim 2 \times 10^4$ s. This gives enough time for some telescopes, e.g. CTA (Inoue et al. 2013), MAGIC (Albert et al. 2007), H.E.S.S. (Aharonian et al. 2009), VERITAS (Acciari et al. 2011), to carry out follow-up observations.

(4) In the *Binary Case*, the strongest EIC emission is expected when $d \sim 10^{14} - 10^{16}$ cm. Therefore, observations can probe the existence and properties of a possible luminous companion in this distance range, as long as electrons are hot at radius $r \sim d$. We note that, in a possible binary Population III (Pop III) star system, the luminosity of the companion star could be as high as 10^{40} erg/s (Heger & Woosley 2002). A Pop III GRB could also have a higher jet kinetic energy $E_{j,54} = 10$ (Suwa & Ioka 2011). If a GRB happens in a Pop III binary system⁹ where the separation between stars is $d = 10^{15}$ cm, under our fiducial parameters, we expect $N_{EIC}^{iso} \simeq 2 \times 10^{53}$ at $\nu_p/(1+z) \sim 8/(1+z)$ GeV,

⁹ The multiplicity and binary separation distribution of Pop III stars are largely unknown. By simulating the growth and evolution of Pop III stellar systems in a sample ($N = 10$) of minihalos, Stacy & Bromm (2013) find a binary fraction of $\sim 35\%$ (at birth) and that the binary separation (at birth) peaks at 10^2 AU. The subsequent evolution of these binary systems is still unexplored.

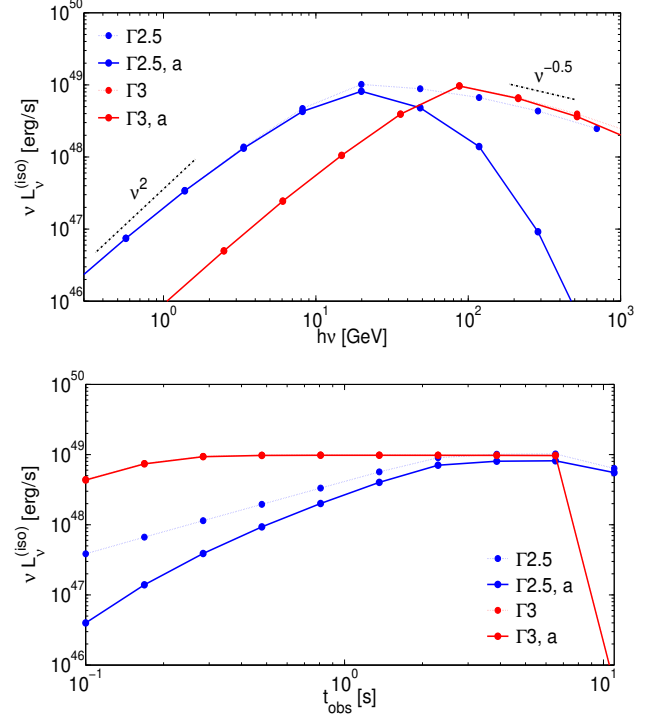


FIG. 8.— Spectra at $t_{obs} = 10$ s (upper panel) and lightcurves at ν_p (lower panel) in the *Cluster Case*, using different bulk LFs. We show the difference between calculations with/without pair-production absorption by using dotted/solid lines (“a” means absorption is considered). Absorption is usually not important in this case, due to large r_{eff} . Considering absorption (solid lines), the total EIC energy is $E_{EIC} = 7.4 \times 10^{49}$ (blue), 1.0×10^{50} (red) erg. The spectra show $\nu L_\nu \propto \nu^2$ below ν_p and $\propto \nu^{-0.5}$ above ν_p , plus additional high energy softening caused by absorption. The scaled parameters $E_{j,54}$, $T_{j,1}$, $\gamma_{i,2}$, $T_{4,7}$, $L_{b,39}$, $r_{max,15}$, $n_{*,4}$, R_{pc} are all set to 1. Powerlaw index $p = 2.2$.

which means a photon fluence of $\sim 10^{-7}$ cm⁻² at redshift $z = 15$ and that could be observed by future large telescopes.

(5) In the *Wind Case*, EIC emission is usually weak ($E_{EIC} \sim 10^{49}$ erg), but since $E_{EIC} \propto L_b \dot{M}$ (Eq.29), this case is worth considering because of two possible enhancement channels. First, there might be a persistent (months to years) and strong ($10^{-3} \sim 1 M_\odot/yr$) pre-burst mass loss, as seen in some Type Ibc and all Type II supernovae (SNe, e.g. Foley et al. 2007; Smartt 2009; Kiewe et al. 2012). We also note that the strong mass loss might not be isotropic¹⁰ and hence could leave no footprints on the afterglow dynamics. Second, an unusually high stellar luminosity might be produced by, e.g. a SN slightly earlier than the GRB, or a hot cocoon¹¹ surrounding the jet.

(6) In the *Star Cluster Case*, we emphasize the importance of EIC radiation from the external shock (ES), because we have a better understanding of the ES than of the internal shock in that the standard (low energy) GRB afterglows are most likely due to synchrotron radi-

¹⁰ For example, due to the fast rotation of the progenitor, most of the gas could be ejected near the equatorial plane.

¹¹ See Kumar & Smoot (2014) for the EIC scattering of the hot cocoon radiation by the GRB jet.

tion from the ES-accelerated electrons (e.g. Piran 2004). However, the uncertainties of the EIC emission from ES come from the jet dynamical evolution, which depends on circum-burst number density and jet power. We predict photon fluence from 10^{-6} cm^{-2} (forward shock, $\sim 30 \text{ GeV}$) to 10^{-5} cm^{-2} (reverse shock, $\sim 10 \text{ GeV}$) at redshift $z = 1$, using our fiducial parameters. Future large telescopes should be able to constrain the properties of the cluster.

(7) Another interesting application is the IC scattering of the Cosmic Microwave Background (CMB) at high redshift by Pop III GRB jets. The earliest Pop III stars form in minihalos of mass $\sim 10^6 M_\odot$ at redshift $z \sim 20 - 30$ (Bromm 2013). The CMB photon number density is

$$n_{\text{CMB}} \simeq aT^4/(2.7kT) = 3.3 \times 10^6[(1+z)/20]^3 \text{ cm}^{-3} \quad (50)$$

where we have used the CMB temperature $T = 2.7(1+z) = 54K(1+z)/20$ (i.e. $\epsilon_0 = 4.7 \times 10^{-3} \text{ eV}$). The forward shock (FS) is highly relativistic at deceleration radius, and electrons are accelerated to LF $\gamma_e = 1.8 \times 10^5$ (using $\epsilon_e = 0.1$, and $\Gamma_{\text{dec}} = 100$). Therefore, EIC emission from the FS could be observed at $0.8 \text{ GeV } \Gamma_{\text{dec},2}^4$. If we use a jet kinetic energy $E_j = 10^{55} \text{ erg}$ (isotropic equivalent) and a uniform circum-burst medium density of $n = 100 \text{ cm}^{-3}$, we get the deceleration radius $r_{\text{dec}} \simeq 10^{17} \text{ cm}$ (Eq.37). The total (isotropic) number of EIC photons from FS is

$$\begin{aligned} N_{\text{EIC}}^{\text{FS}} &\simeq (\tau_{\text{FS}} n_{\text{CMB}} 4\pi r^3/3)|_{r=r_{\text{dec}}} \\ &\simeq 3.0 \times 10^{52} [(1+z)/20]^3 n_2 r_{\text{dec},17}^4 \end{aligned} \quad (51)$$

Since $N_{\text{EIC}}^{\text{FS}}$ strongly depends on r_{dec} , a more accurate calculation of the dynamical evolution is needed. Using $N_{\text{EIC}}^{\text{FS}} = 3 \times 10^{52}$, we expect a photon fluence of $\sim 5 \times 10^{-9} \text{ cm}^{-2}$ at $\sim 1 \text{ GeV}$ from redshift 20.

4. DISCUSSION

In this section, we discuss some potential issues of the EIC emission proposed in this paper.

(1) We note that high energy γ -rays can't propagate through cosmological distances, due to pair production with extragalactic background light (consisting mostly of cosmic infrared, optical and UV backgrounds). Photons of energy $\geq 100 \text{ GeV}$ can only be observed from nearby ($z < 1$) GRBs (Gilmore et al. 2012). However, GRBs with low bulk LF $\Gamma \leq 300$ will mostly produce $\leq 10 \text{ GeV}$ photons, which could be observed at high redshift.

(2) In the *Binary Case*, the EIC luminosity is only significant when the binary separation is large ($d \geq 10^{14} \text{ cm}$). Orbital separation distribution derived from spectroscopic and direct imaging studies are inevitably biased by selection effects and measurement limitations. By measuring radial velocities, Sana et al. (2012) derived (after completeness corrections) the distribution of orbital periods $f(\log P) \propto (\log P)^{-0.55}$ for $P = 1.4 - 3200 \text{ d}$ by analyze the O star population of six nearby Galactic open clusters. Also by measuring radial velocities, Kobulnicky et al. (2014) estimated $f(\log P) \propto (\log P)^{-0.22}$ for $P = 1.4 - 2000 \text{ d}$ in the Cygnus OB2 Association. Despite the discrepancy (and also uncertainties), both of them pointed out that about 10% of the binary systems have periods $P > 10^3 \text{ d}$, which corresponds

to $d \simeq 10^{14} \text{ cm}$. An even greater uncertainty comes from the unknown nature of GRB progenitors, which may not be O stars (Woosley 1993; MacFadyen & Woosley 1999). From our calculations, early observations of GRB high energy γ -ray emission is sensitive in probing the possible companion star at $d \sim 10^{14} - 10^{16} \text{ cm}$.

(3) In the *Star Cluster Case*, the EIC luminosity depends on the number density of massive stars at the time when the GRB occurs. There are large uncertainties in the first few Myr of the star clusters' evolution (see e.g. Portegies Zwart et al. 2010), especially in the so-called Gas Expulsion Stage (GES) during which the residual gas in the cluster is blown away by stellar winds or outflows. The loss of mass during GES will cause the cluster to expand and the shallower potential well may allow a fraction of the stars (especially the ones at outer radius) to escape. Therefore, the overall stellar number density drops with time. Long GRBs are concentrated on the very brightest regions of actively star-forming galaxies, where young massive clusters are particularly abundant (Fruchter et al. 2006). However, little is known about the very nearby ($\sim 1 \text{ pc}$) environment around the long GRB progenitors, and it is unclear whether the stars escaped¹² from the clusters. The EIC signal proposed in this paper could potentially give us some hint. For example, an upper limit of $L_{\text{EIC}} < 10^{49} \text{ erg/s}$ will constrain the number density of massive ($> 20 - 30 M_\odot$) stars to be $n_* < 10^4 \text{ pc}^{-3}$.

(4) There are a few potential issues in our numerical procedures developed in Section 2. (a) Electrons' LF distribution may not be a single powerlaw. Due to synchrotron, synchrotron-self-Compton, or EIC cooling, there's a cooling LF γ_c above which electrons' distribution turns softer. The resulting EIC spectrum at energy higher than $\Gamma \gamma_c m_e c^2$ will be softer than our prediction, but the total EIC energy will not change much, as long as $\gamma_c > \gamma_i$. (b) Electron's LF distribution is evolving with time, i.e. γ_i, γ_c and possibly the powerlaw index p are all functions of time (or radius). In principle, by convolving the time dependent LF distribution with single particle emission, we can calculate the EIC emission to a higher degree of accuracy. However, since we are not yet sure where the internal shock (IS) is active and how long will electrons stay hot (Kumar & Zhang 2014), such a detailed calculation is left for possible future investigation. Instead, constant γ_i and p are used at all radius. Since the IS is mildly relativistic and GRB afterglow modeling often shows that electrons share a fraction $\epsilon_e \simeq 0.1$ of fluid's internal energy (e.g. Panaitescu & Kumar 2001), we use $\gamma_i = 10^2$ for IS-accelerated electrons. We use first-order-Fermi accelerated electron powerlaw index $p = 2.2$ throughout the paper. As we show in Section 3.2 (Fig.6), by using a constant γ_i at all radius, we are making an assumption that electrons are hot near the radius r_{eff} where most scatterings happen.

(5) Lastly, we estimate the possible contribution of the EIC emission to the extragalactic γ -ray background (EGB) around 100 GeV , by the FS channel or when GRBs have large LF (e.g. $\Gamma \geq 500$). We optimistically estimate the average (isotropic) EIC energy

¹² Hammer et al. (2006) found GRB 980425 (the nearest GRB at $z = 0.008$, e.g. Galama et al. 1998) to be $\sim 800 \text{ pc}$ away from the nearby massive star-forming region.

around 100 GeV from one GRB to be $E_{EIC} = 10^{51}$ erg . The average (observed) GRB rate in the local ($z < 1$) Universe is estimated by Wanderman & Piran (2010) to be $\bar{\rho} \sim 3 \text{ Gpc}^{-3} \text{ yr}^{-1}$. We integrate over the local Universe to $R_{max} = 4 \text{ Gpc}$ and estimate the intensity of EGB contributed by the EIC channel to be $I_{EGB} \simeq E_{EIC} \bar{\rho} R_{max} / 4\pi \simeq 2 \times 10^{-6} \text{ MeV cm}^{-2} \text{ s}^{-1} \text{ sr}^{-1}$. The EGB at 100 GeV observed by Fermi LAT is $\sim 10^{-4} \text{ MeV cm}^{-2} \text{ s}^{-1} \text{ sr}^{-1}$ (Abdo et al. 2010). Therefore, the EIC channel in GRBs could (at most) contribute a small fraction of EGB. The possible contributions from other GRB channels are estimated by Casanova et al. (2007).

5. CONCLUSIONS

GRB progenitors may be surrounded by a significant external photon field (EPF), due to the existence of a massive companion star (*Case I*), a strong stellar wind (*Case II*), or a dense star cluster (*Case III*). We calculate the IC scattering of the EPF (i.e. EIC emission) by the hot electrons in the GRB jet, which could be accelerated by internal dissipation process or the external shock (ES). We have presented in this work EIC lightcurves and spectra. Note that we call the internal dissipation process that produces the prompt γ -rays as “internal shock” (IS) only for simplicity, but our model is independent of the detail process.

In each case, the EPF-contributing star(s) are assumed to have bolometric luminosity 10^{39} erg/s and effective temperature 5×10^4 K . The GRB jet is assumed to have total kinetic energy 10^{54} erg (isotropic equivalent), duration $T_j = 10$ s and bulk Lorentz factor (LF) $\Gamma = 300$. We assume that electrons are accelerated by IS to a powerlaw distribution with minimum LF $\gamma_i = 10^2$ and index $p = 2.2$. We take into account the absorption of high energy photons caused by pair production with the prompt γ -rays. The EIC spectrum peaks at $\nu_p \sim 10$ GeV for our fiducial parameters. However, for a faster jet $\Gamma = 10^3$, we get $\nu_p \sim 100$ GeV . The EIC spectrum below ν_p is $\nu L_\nu \propto \nu^2$ and $\propto \nu^{-0.5}$ above ν_p ; pair production softens the spectrum at high energies (above the threshold for e^\pm production). In *Case III*), signifi-

cant EIC emission also comes from electrons accelerated by ES, where we use $\epsilon_e = 0.1$ as the fraction of internal energy shared by hot electrons in the shocked regions.

In *Case I*), using binary separations $10^{14} - 10^{16}$ cm , we get EIC luminosities of $10^{47} - 10^{50}$ erg/s (the effect of pair production on high energy photon luminosity is included in this and all calculations below), peaking at separation 10^{15} cm . In *Case II*), soft photons originally from the progenitor star are scattered first by the electrons in the stellar wind and again by the jet. Using a W-R-star mass loss rate $10^{-5} M_\odot/\text{yr}$ and wind velocity 10^8 cm/s , we get an EIC luminosity of 10^{48} erg/s . In *Case III*), we assume that stars in the cluster create a uniform EPF. Electrons in the jet are accelerated by both IS and ES. We include both the reverse shock (RS) and forward shock (FS) in ES. Using stellar number density 10^4 pc^{-3} and cluster radius 1 pc , we get EIC luminosities of 10^{49} erg/s from IS, and 10^{49} erg/s from external reverse shock and 10^{46} erg/s from external forward shock. The EIC emission from IS lasts for $t_{obs} \simeq T_j \sim 10$ s , but that from ES lasts longer, approximately 200 s from RS and 2×10^4 s from FS.

We note that EIC emission from IS relies on the assumption that electrons are hot at the right radius r_{eff} : $\sim d$ (the binary separation, *Case I*), $\sim r_{tr}$ ($\sim 3 \times 10^{14}$ cm , the radius where the jet becomes transparent, *Case II*) and $10^{16} \text{ cm } r_{max,16}$ (the maximum radius electrons stay hot, *Case III*). In addition, EIC emission from ES strongly depends on the dynamical evolution of the jet.

Generally, a photon fluence of $10^{-7} - 10^{-5} \text{ cm}^{-2}$ at 10 - 100 GeV is expected. Future observations can put constraints on: (1) the existence of such EPFs as described in this paper and hence on the nature of GRB progenitors; (2) the radius where the jet internal dissipation process accelerates electrons.

The authors thank M. Milosavljević, P. Crumley, R. Santana, R. Hernández for helpful discussions. G.F.S. acknowledges support through his Chaire d’Excellence Université Sorbonne Paris Cité and the financial support of the UnivEarthS Labex program at Université Sorbonne Paris Cité (ANR-10-LABX-0023 and ANR-11-IDEX-0005-02).

REFERENCES

- Abdo, A. A., Ackermann, M., Ajello, M., et al. 2010, ApJ, 720, 435
- Acciari, V. A., Aliu, E., Arlen, T., et al. 2011, ApJ, 743, 62
- Ackermann, M., Ajello, M., Asano, K., et al. 2013, ApJS, 209, 11
- Aharonian, F. A., & Atoyan, A. M. 1981, Ap&SS, 79, 321
- Aharonian, F., Akhperjanian, A. G., Barres de Almeida, U., et al. 2009, A&A, 495, 505
- Albert, J., Aliu, E., Anderhub, H., et al. 2007, ApJ, 667, 358
- Band, D., Matteson, J., Ford, L., et al. 1993, ApJ, 413, 281
- Blandford, R. D., & McKee, C. F. 1976, Physics of Fluids, 19, 1130
- Blumenthal, G. R., & Gould, R. J. 1970, Reviews of Modern Physics, 42, 237
- Bromm, V. 2013, Reports on Progress in Physics, 76, 112901
- Casanova, S., Dingus, B. L., & Zhang, B. 2007, ApJ, 656, 306
- Chevalier, R. A., Li, Z.-Y., & Fransson, C. 2004, ApJ, 606, 369
- Crowther, P. A. 2007, ARA&A, 45, 177
- Dermer, C. D., & Schlickeiser, R. 1993, ApJ, 416, 458
- Espinoza, P., Selman, F. J., & Melnick, J. 2009, A&A, 501, 563
- Fan, Y.-Z., Piran, T., Narayan, R., & Wei, D.-M. 2008, MNRAS, 384, 1483
- Foley, R. J., Smith, N., Ganeshalingam, M., et al. 2007, ApJ, 657, L105
- Fruchter, A. S., Levan, A. J., Strolger, L., et al. 2006, Nature, 441, 463
- Galama, T. J., Vreeswijk, P. M., van Paradijs, J., et al. 1998, Nature, 395, 670
- Ghisellini, G., Lazzati, D., Celotti, A., & Rees, M. J. 2000, MNRAS, 316, L45
- Giannios, D. 2008, A&A, 488, L55
- Gilmore, R., & Ramirez-Ruiz, E. 2010, ApJ, 721, 709
- Gilmore, R. C., Somerville, R. S., Primack, J. R., & Domínguez, A. 2012, MNRAS, 422, 3189
- Gruber, D., Goldstein, A., Weller von Ahlefeld, V., et al. 2014, ApJS, 211, 12
- Guetta, D., & Granot, J. 2003, MNRAS, 340, 115
- Hammer, F., Flores, H., Schaerer, D., et al. 2006, A&A, 454, 103
- Heger, A., & Woosley, S. E. 2002, ApJ, 567, 532
- Hjorth, J., Sollerman, J., Møller, P., et al. 2003, Nature, 423, 847
- Inoue, S., Granot, J., O’Brien, P. T., et al. 2013, Astroparticle Physics, 43, 252
- Kiewe, M., Gal-Yam, A., Arcavi, I., et al. 2012, ApJ, 744, 10

- Kobayashi, S. 2000, ApJ, 545, 807
 Kobulnicky, H. A., Kiminki, D. C., Lundquist, M. J., et al. 2014, arXiv:1406.6655
 Kumar, P., & Smoot, G. F. 2014, arXiv:1402.2656
 Kumar, P., & Zhang, B. 2014, arXiv:1410.0679
 Lada, C. J., & Lada, E. A. 2003, ARA&A, 41, 57
 Langer, N. 2012, ARA&A, 50, 107
 Lazzati, D., Ghisellini, G., Celotti, A., & Rees, M. J. 2000, ApJ, 529, L17
 MacFadyen, A. I., & Woosley, S. E. 1999, ApJ, 524, 262
 MacFadyen, A. I., Woosley, S. E., & Heger, A. 2001, ApJ, 550, 410
 Madau, P., & Phinney, E. S. 1996, ApJ, 456, 124
 Mason, B. D., Hartkopf, W. I., Gies, D. R., Henry, T. J., & Hessel, J. W. 2009, AJ, 137, 3358
 Massey, P., & Hunter, D. A. 1998, ApJ, 493, 180
 Matzner, C. D. 2003, MNRAS, 345, 575
 Mészáros, P. 2006, Reports on Progress in Physics, 69, 2259
 Panaitescu, A., & Kumar, P. 2001, ApJ, 560, L49
 Piran, T. 2004, Reviews of Modern Physics, 76, 1143
 Portegies Zwart, S. F., McMillan, S. L. W., & Gieles, M. 2010, ARA&A, 48, 431
 Ramirez-Ruiz, E. 2004, MNRAS, 349, L38
 Sana, H., de Mink, S. E., de Koter, A., et al. 2012, Science, 337, 444
 Smartt, S. J. 2009, ARA&A, 47, 63
 Stacy, A., & Bromm, V. 2013, MNRAS, 433, 1094
 Suwa, Y., & Ioka, K. 2011, ApJ, 726, 107
 Uhm, Z. L. 2011, ApJ, 733, 86
 Wanderman, D., & Piran, T. 2010, MNRAS, 406, 1944
 Woosley, S. E. 1993, ApJ, 405, 273
 Woosley, S. E., & Bloom, J. S. 2006, ARA&A, 44, 507
 Zhang, B. 2014, International Journal of Modern Physics D, 23, 30002
 Zinnecker, H., & Yorke, H. W. 2007, ARA&A, 45, 481

APPENDIX

There are two potential pair-production channels that could absorb the high energy part (10 GeV - 100 GeV) of the EIC photons. (1) In the lab frame, the EPF (~ 10 eV) will interact with ~ 100 GeV photons. We show below that this channel is usually not important. (2) In the jet comoving frame, the GRB prompt emission (~ 1 keV) will interact with ~ 1 GeV photons (~ 100 GeV in the lab frame). We consider this channel in detail, following Madau & Phinney (1996); Gilmore & Ramirez-Ruiz (2010), and this channel is included in our numerical calculation (Section 2).

Absorption by EPF Itself

The only concern here is for photons of energy ≥ 100 GeV. The optical depth of pair production is

$$\tau_{\gamma\gamma} \simeq n_{\gamma} \sigma l \quad (\text{A1})$$

where l is the path length of the high energy γ -ray through the EPF, n_{γ} is the number density of field photons near the energy of maximum cross section, and $\sigma \simeq 0.1\sigma_T$ is the approximate cross section.

In the *Binary Case*, most scatterings happen at radius $r \sim d$, so we have

$$\tau_{\gamma\gamma}^{(1)} \simeq \frac{L_b}{4\pi(d^2 + d^2)\epsilon_0 c} \left(1 - \frac{\sqrt{2}}{2}\right) \sigma d = 1.6 \times 10^{-2} \frac{L_{b,39}}{d_{14}\epsilon_{0,1}} \quad (\text{A2})$$

In the *Wind Case*, most scatterings happen at radius $r \sim r_{tr}$ (see Eq.21 and 26), so we have

$$\tau_{\gamma\gamma}^{(2)} \simeq \frac{L_b \tau_{wind}(r_{tr})}{4\pi r_{tr}^2 \epsilon_0 c} \sigma r_{tr} = 2 \times 10^{-6} \frac{\Gamma_{2.5} L_{b,39} \dot{M}_{-5}}{E_{j,54} \eta_{KN} \epsilon_{0,1} v_8} \quad (\text{A3})$$

In the *Star Cluster Case*, EIC photons need to penetrate the whole cluster that has radius $R = 1pc R_{pc}$, so we have

$$\tau_{\gamma\gamma}^{(3)} \simeq \frac{n_* L_b R}{\epsilon_0 c} \sigma R = 4.5 \times 10^{-1} \frac{n_{*,4} L_{b,39} R_{pc}^2}{\epsilon_{0,1}} \quad (\text{A4})$$

These are upper limits, since some EPF photons are either offset from the maximum cross section energy or at energy lower than the threshold. Anyway, the absorption is only important in *Binary Case* when $d \lesssim 10^{12}$ cm and in *Star Cluster Case* when $R \gtrsim 1$ pc. Under these conditions, there will be a spectral cut off at $> \sim 100$ GeV. The absorption is not important in *Wind Case*. A more detailed calculation is given by Gilmore & Ramirez-Ruiz (2010).

Absorption by GRB Prompt Emission

In the jet comoving frame, a high energy EIC photon of frequency ν' is surrounded by low energy photons (frequency ν'_l), which can be described by the so-called Band function (Band et al. 1993). We simplify the Band function as a broken powerlaw of indexes α_1 and α_2 , below and above the break frequency ν_b . From the prompt emission bolometric isotropic luminosity L_{γ} , and the radius r where the low energy photons are produced, we get the comoving-frame specific number density

$$n'_{\nu'_l}(r) = \frac{L_{\gamma}}{4\pi r^2 c h \nu_b^2} \left(\frac{1}{\alpha_1 + 2} - \frac{1}{\alpha_2 + 2} \right)^{-1} \cdot \begin{cases} (\nu'_l/\nu'_b)^{\alpha_1} & \text{if } \nu'_l < \nu'_b \\ (\nu'_l/\nu'_b)^{\alpha_2} & \text{if } \nu'_l > \nu'_b \end{cases} \quad (\text{A5})$$

where $\nu'_b = \nu_b/\Gamma$ is the break frequency in the comoving frame. The pair-production threshold is

$$h\nu'_{th} = \frac{2(m_e c^2)^2}{h\nu'(1 - \cos\theta'_l)} \quad (\text{A6})$$

where θ'_l is the angle between high(ν') and low(ν'_l) energy photons' momentum vectors. The cross section for pair production is (Madau & Phinney 1996)

$$\sigma_{\gamma\gamma}(\nu', \nu'_l, \theta'_l) = \frac{3\sigma_T}{16}(1 - q^2) \left[(3 - q^4) \ln \frac{1+q}{1-q} + 2q(q^2 - 2) \right] \quad (\text{A7})$$

where $q = \sqrt{1 - \nu'_{th}/\nu'_l}$. Assuming that low energy photons are moving isotropically in the jet comoving frame, we get the mean free path

$$l_{\gamma\gamma}^{-1}(\nu', r) = \frac{1}{2} \int_{-1}^1 d(\cos\theta'_l)(1 - \cos\theta'_l) \int_{\nu'_{th}}^{\infty} d\nu'_l n'_{\nu'_l} \sigma_{\gamma\gamma} \quad (\text{A8})$$

Then the pair-production optical depth is the comoving dynamical timescale divided by the mean time interval between two collisions, i.e.

$$\tau_{\gamma\gamma}(\nu', r) = \frac{r}{\Gamma l_{\gamma\gamma}(\nu', r)} \quad (\text{A9})$$

Therefore, only a fraction $e^{-\tau_{\gamma\gamma}}$ of the EIC photons in Eq.(13) can escape. A simple estimate of the pair-production optical depth is

$$\tau_{\gamma\gamma} \simeq 0.1\sigma_T \frac{L_\gamma/4}{4\pi r^2 c h \nu'_{th} \Gamma^2} \frac{r}{\Gamma} \simeq 0.65 \frac{L_{\gamma,52}(h\nu/10\text{GeV})}{r_{15} \Gamma_{2.5}^4} \quad (\text{A10})$$

where we assume 1/4 of all the prompt γ -rays contribute to the absorption of high energy photons. We can see: (1) $\tau_{\gamma\gamma}$ is very sensitive to the bulk Lorentz factor (we have used $\Gamma = 300\Gamma_{2.5}$); (2) most absorption happens at small radius ($r_{15} \leq 1$) and high frequency ($h\nu \geq 10 \text{ GeV}$).